DOI: 10.1002/ejic.201100724

# Cyano- and Aqua-Coordinated Diruthenium(III) Complexes with Oxo-Bis(acetato) Bridge: Preparation and Steric and Electronic Structures

Hua-Xin Zhang,*[a,b] Kiyoshi Tsuge,[b] Yoichi Sasaki,*[a,b] Masatoshi Osawa,[a] and Masaaki Abe[c]

**Keywords:** Ruthenium / Bridging ligands / Cyano complexes / Electronic structure / Charge transfer

Three new μ-oxo-bis(μ-acetato)diruthenium(III) complexes, *trans*(μ-O,OH$_2$)-[Ru$_2$(μ-O)(μ-CH$_3$COO)$_2$(bpy)$_2$(H$_2$O)$_2$][PF$_6$]$_2$·3H$_2$O ([**1**][PF$_6$]$_2$·3H$_2$O; bpy = 2,2′-bipyridine), *trans*(μ-O,CN)-[{Ru$_2$(μ-O)(μ-CH$_3$COO)$_2$(bpy)$_2$}$_2${μ-Ag(CN)$_2$}{μ-Ag$_2$(CN)$_3$}]-[Ag(CN)$_2$][Ag$_2$(CN)$_3$](CH$_3$CN)$_4$(CH$_2$Cl$_2$) (**2**), and *cis*(μ-O,CN)-[Ru$_2$(μ-O)(μ-CH$_3$COO)$_2$(bpy)$_2$(CN)$_2$]·CH$_3$OH·H$_2$O ([**3**]·CH$_3$OH·H$_2$O), have been prepared and their X-ray crystal structures determined. Whereas [**1**]$^{2+}$ and **3** are discrete species, **2** is a polymer in which the Ag–CN groups act as bridges through Ru–CN(or NC)–Ag linkages. The discrete complexes dissolve in common solvents, but **2** is only slightly soluble in acetonitrile and dimethyl formamide (DMF) to give fragmented species (denoted as **2′**) in solution. Redox waves of **3** were observed at –0.83 ($E_{pc}$) and +0.76 V ($E_{1/2}$) versus Ag/AgCl in a solution of 0.1 M *n*Bu$_4$NPF$_6$ in CH$_2$Cl$_2$, which correspond to the Ru$_2^{II,III}$/Ru$_2^{III,III}$ and Ru$_2^{III,III}$/Ru$_2^{III,IV}$ processes, respectively. The corresponding redox couples ($E_{1/2}$) of [**1**]$^{2+}$ were observed at –0.31 and +0.76 V in 0.1 M NaClO$_4$ aqueous solution. Significantly more negative potentials of the Ru$_2^{II,III}$/Ru$_2^{III,III}$ couple for the two cyano complexes ($E_{1/2}$ = –0.77 V for **2′**) are noted. Complexes [**1**]$^{2+}$, **2′**, and **3** exhibit strong visible absorption bands at $\lambda_{max}$ = 566 nm ($\varepsilon$ = 12600 M$^{-1}$cm$^{-1}$; in H$_2$O), 636 nm (21000 M$^{-1}$cm$^{-1}$; in acetonitrile), and 558 nm (18000 M$^{-1}$cm$^{-1}$; in H$_2$O), respectively. Density functional theory (DFT) molecular orbital calculations have been carried out for [**1**]$^{2+}$, *trans*(μ-O,CN)-[Ru$_2$(μ-O)(μ-CH$_3$COO)$_2$(bpy)$_2$(CN)$_2$] (**2a**, a model compound for **2′**), **3**, [Ru$_2$(μ-O)(μ-CH$_3$COO)$_2$(py)$_6$]$^{2+}$ ([**4**]$^{2+}$), and *trans*(μ-O,py)-[Ru$_2$(μ-O)(μ-CH$_3$COO)$_2$(bpy)$_2$(py)$_2$]$^{2+}$ ([**5**]$^{2+}$; py = pyridine). It was revealed that the frontier orbitals of these complexes are dominated by the Ru(dπ)–μ-O(pπ) type π systems. For the cyano complexes, energies of these π-type MOs are lifted up by the interaction with CN$^-$, so that the energy difference with the upper bpy π* orbitals becomes smaller. Thus, whereas the visible absorption bands of [**1**]$^{2+}$, [**4**]$^{2+}$, and [**5**]$^{2+}$ are ascribed to the transitions within the π system metal-to-metal charge transfer (MMCT), those of **2′** and **3** are ascribed to the HOMO-to-ligand π* (bpy) transition metal-to-ligand charge transfer (MLCT) and to the mixture of MMCT and MLCT (HOMO–1 to π*), respectively.

## Introduction

Oxo-bridged di- and polynuclear metal complexes are among the most frequently found structural motif of the aggregation of metal ions.[1–3] In particular, those of second and third transition-metal ions are relatively stable and characterized by their appreciably stronger π-type [(metal)dπ–(O)pπ] interactions relative to those of the first transition-metal ions.[3a–3f,3h] The dπ–pπ interactions have some important consequences on electronic, magnetic, and redox properties, and therefore the oxo-bridged heavy transition-metal complexes show notably different characteristics from those of their first transition-metal analogues. The electronic structures of the oxo-bridged second and third transition-metal complexes are still understood on a rather qualitative basis, however, and the role of nonbridging ligands is less focused.

Among the oxo-bridged heavy transition-metal complexes, those with ruthenium-containing units such as Ru$_2$(μ-O)(μ-RCOO)$_2$ and Ru$_3$(μ$_3$-O)(μ-RCOO)$_6$ are the most extensively studied.[3a–3e,4,5] This is because these complexes show characteristic visible electronic transitions and multistep multielectron redox behavior based on the dπ–pπ interactions. Also, the diruthenium unit is considered a structural model of the diiron and dimanganese analogues found in biological systems.[1,2,4] Thus, further detailed study of the electronic structures of these ruthenium complexes is important not only for their own sake but also for oxo-bridged complexes in general, in particular to understand the role of nonbridging ligands. Replacement of the nonbridging ligand in the di- and triruthenium units has made it possible to study the chemistry of these interesting structural motifs in a somewhat systematic way. Nevertheless, the electronic structures have been discussed mostly on

[a] Catalysis Research Center Hokkaido University, Sapporo 001-0021, Japan
Fax: +81-11-706-9125
E-mail: zhang@sci.hokudai.ac.jp, ysasaki@sci.hokudai.ac.jp
[b] Division of Chemistry, Graduate School of Science, Hokkaido University, Sapporo 060-0810, Japan
[c] Department of Applied Chemistry, Graduate School of Engineering, Kyushu University, Nishi-ku, Fukuoka 819-0395, Japan

Supporting information for this article is available on the WWW under http://dx.doi.org/10.1002/ejic.201100724.

  

the basis of the qualitative dπ–pπ interaction scheme.[5] Although the ligands with strong π-interacting character such as CO and $CN^-$ may play a significant role, no quantitative study has been reported except for the significant effect of CO on the triruthenium unit to stabilize the lower oxidation state.[3d] To date the cyano ligand has never been introduced to these oxo-di- and triruthenium units. In this study, we focus our attention on the role of the cyano ligand in the electronic structures of the diruthenium complex unit.

Diruthenium complexes, $[Ru_2(\mu\text{-}O)(\mu\text{-}RCOO)_2(\mathbf{L})_6]^{n+}$, in which **L** is a monodentate ligand or a monodentate "fragment" of the di- or polynuclear ligands, have been the subject of detailed systematic study in the past few decades.[4] The Ru–Ru interaction has been discussed on the basis of the Ru(dπ)–O(pπ) interactions within the $Ru_2(\mu\text{-}O)(\mu\text{-}RCOO)_2$ core.[5] Sequential one-electron redox processes are often observed that involve the five oxidation states $Ru_2^{II,II}$/$Ru_2^{II,III}$/$Ru_2^{III,III}$/$Ru_2^{III,IV}$/$Ru_2^{IV,IV}$.[6] The proton-coupled redox behavior as characterized by a significant positive shift of the reduction potentials that involve lower oxidation states has been observed in acidic solutions.[7] Also, the $Ru_2^{III,III}$ complexes are known to show a strong absorption band around 600 nm that has been assigned to the n (or π) → π* transition within the Ru(dπ)–O(pπ) molecular orbitals.[5] For the complexes with aromatic nitrogen bases such as pyridine, imidazole, and their derivatives at nonbridging coordination sites, linear correlations between the p$K_a$ values of the coordinated nitrogen bases and the transition energies of the visible absorption bands has been pointed out.[8] The p$K_a$ value of the ligand is not a parameter that is directly related to the π-type interaction, however, and further insight into the electronic structure including the influence of the nonbridging ligands is yet to be explored. It should also be noted that additional visible absorption bands are often observed at higher-energy regions that are tentatively assigned to the MLCT transitions that involve π* orbitals of aromatic ligands such as 2,2′-bipyridine and 1,10-phenanthrolline, thus indicating that the Ru(dπ)–O(pπ) molecular orbitals are rather close in energy to the ligand orbitals.

The purpose of this work is to show a more precise picture of the electronic structure of the diruthenium complexes with the $Ru_2(\mu\text{-}O)(\mu\text{-carboxylato})_2$ core. The types of nonbridging ligands used so far are aromatic and aliphatic nitrogen bases, phosphanes, and some solvent molecules.[4–9] The cyanide ion ($CN^-$) is known as a ligand that has a significant π back-bonding character as well as a strong σ-donating ability[10] and is expected to have a significant influence on the π system that characterizes the electronic structure of the $Ru_2(\mu\text{-}O)(\mu\text{-carboxylato})_2$ core. In this study, new cyano complexes of the type $[Ru_2(\mu\text{-}O)(\mu\text{-}CH_3COO)_2(bpy)_2(CN)_2]$ (bpy = 2,2′-bipyridine) have been prepared both in the *trans*(μ-O,CN) and the *cis*(μ-O,CN) forms. Whereas the former isomer has been isolated as an extended polymer, *trans*(μ-O,CN)-$[\{Ru_2(\mu\text{-}O)(\mu\text{-}CH_3COO)_2(bpy)_2\}_2\{\mu\text{-}Ag(CN)_2\}\{\mu\text{-}Ag_2(CN)_3\}][Ag(CN)_2][Ag_2(CN)_3](CH_3CN)_4(CH_2Cl_2)$ (**2**), the latter has been obtained as a discrete species, *cis*(μ-O,CN)-$[Ru_2(\mu\text{-}O)(\mu\text{-}CH_3COO)_2(bpy)_2(CN)_2]$ (**3**). In addition to the cyano complexes, an aqua complex *trans*(μ-O,$OH_2$)-$[Ru_2(\mu\text{-}O)(\mu\text{-}CH_3COO)_2(bpy)_2(H_2O)_2]^{2+}$ ($[\mathbf{1}]^{2+}$) has also been isolated. As expected, these new complexes have provided useful information on the stereochemistry and redox and spectroscopic properties of μ-oxo-di-μ-carboxylate diruthenium complexes. With the aid of the molecular orbital calculations, we have now unambiguously revealed the detailed electronic structure of the diruthenium complexes and the nature of the visible electronic transitions. Details of these results are reported in this paper.

## Results and Discussion

### Synthesis of the New Complexes

The general procedures for the preparation of the μ-oxo-bis(μ-acetato)diruthenium complexes that contain pyridyl ligands are briefly summarized as follows. On keeping the solution of $RuCl_3{\cdot}nH_2O$ in the mixed solvent $CH_3COOH/C_2H_5OH/H_2O$ at around 70 °C for 10 min, a red solution was obtained. The complexes with the $Ru_2(\mu\text{-}O)(\mu\text{-}CH_3COO)_2$ unit were prepared by adding appropriate pyridyl ligands to the red solution. For example, when pyridine (py) was added to the solution, the salt of the hexa(pyridine) complex cation, $[Ru_2(\mu\text{-}O)(\mu\text{-}CH_3COO)_2(py)_6]^{2+}$ ($[\mathbf{4}]^{2+}$), was isolated.[4a,5] Upon addition of a mixture of 2,2′-bipyridine (bpy) and pyridine, the salt of mixed bpy–py complex, *trans*(μ-O,py)-$[Ru_2(\mu\text{-}O)(\mu\text{-}CH_3COO)_2(bpy)_2(py)_2]^{2+}$ ($[\mathbf{5}]^{2+}$), was obtained,[5] in which two py ligands are located at *trans* positions to the oxo bridge. The *trans*-to-oxo pyridine ligands of these complexes were easily substituted by other N-heteroaromatic monodentate ligands (**L**) in solution at elevated temperatures. Since the ligands in *cis*-to-oxo sites remain coordinated, a series of the *trans*(μ-O, **L**)-[μ-oxo-bis(μ-acetato)]diruthenium complexes were prepared by the substitution.[6e]

It was recently reported that the aqua complexes, $[Ru_2(\mu\text{-}O)(\mu\text{-}CH_3COO)_2(\mathbf{L})_4(H_2O)_2]^{2+}$ (**L** = py, 4-picoline), are formed in solution from $[Ru_2(\mu\text{-}O)(\mu\text{-}CH_3COO)_2(\mathbf{L})_6]^{2+}$ in an acetone/water mixture (60:40 v/v) after one day.[8] In the present study, the aqua complex, $[Ru_2(\mu\text{-}O)(\mu\text{-}CH_3COO)_2(bpy)_2(H_2O)_2][PF_6]_2{\cdot}H_2O$ ($[\mathbf{1}][PF_6]_2{\cdot}H_2O$), has been successfully isolated by adding bpy to the red precursor solution, as described in the Experimental Section. The isolated complex has been fully identified. Single-crystal X-ray analysis revealed that the aqua ligands occupy the *trans* positions to the oxo bridge (vide infra). These aqua ligands are expected to be more labile than the pyridine ligands in $[\mathbf{5}]^{2+}$ as suggested previously for the aqua complexes *trans*(μ-O,$OH_2$)-$[Ru_2(\mu\text{-}O)(\mu\text{-}CH_3COO)_2(py)_4(H_2O)_2]^{2+}$ prepared in situ.[8] The aqua complex $[\mathbf{1}]^{2+}$ is thus expected to be a good precursor for the preparation of new complexes of the type *trans*(μ-O,**L**′)-$[Ru_2(\mu\text{-}O)(\mu\text{-}CH_3COO)_2(bpy)_2(\mathbf{L}')_2]^{2+}$ (**L**′ = pyridine, imidazole, 4-cyanopyridine, and so forth). In fact, the formation of these complexes was confirmed by the changes in UV/Vis absorption spectra once the **L**′ ligands were added to the aqueous solution of $[\mathbf{1}]^{2+}$.

  

Two new cyano complexes, **2** and **3**, have now been isolated from the aqueous solution of *trans*(μ-O,$CH_3CN$)-$[Ru_2(\mu\text{-}O)(\mu\text{-}CH_3COO)_2(bpy)_2(CH_3CN)_2]^{2+}$ ($[\mathbf{6}]^{2+}$)[11] by adding $KAg(CN)_2$ as a source of $CN^-$. The aqua complex $[\mathbf{1}]^{2+}$ must be the precursor of the cyano complexes, since the acetonitrile ligands in $[\mathbf{6}]^{2+}$ are easily replaced by aqua ligands in aqueous solutions to give $[\mathbf{1}]^{2+}$. The reaction with $KAg(CN)_2$ gave a blue precipitate of **2**, *trans*(μ-O,CN)-$[\{Ru_2(\mu\text{-}O)(\mu\text{-}CH_3COO)_2(bpy)_2\}_2\{\mu\text{-}Ag(CN)_2\}\{\mu\text{-}Ag_2(CN)_3\}][Ag(CN)_2][Ag_2(CN)_3](CH_3CN)_4(CH_2Cl_2)$, in which $Ag(CN)_2^-$ and $Ag_2(CN)_3^-$ ions act as connectors between the diruthenium units at the sites *trans* to the oxo bridge to give an extended solid structure (vide infra). By carrying out the reaction in the presence of $Cl^-$ to remove $Ag^+$ as AgCl, a different cyano complex, **3**, was isolated. Interestingly, the cyano ligands are in the *cis* positions to the oxo bridge, and the bpy ligands chelate between the *cis*- and *trans*-to-oxo sites. Migration of the cyano ligand from the latter to the former site must have taken place during the preparation process.

### Structural Characterization of the New Complexes

Structures of the three complexes were verified by X-ray crystallography. Shown in Figures 1, 2, and 3 are the molecular structures of $[\mathbf{1}]^{2+}$, **2**, and **3**, respectively. Selected bond lengths and angles are given in Tables S1, S2, and S3 of the Supporting Information. As expected, all the complexes have the μ-oxo-bis(μ-acetato)diruthenium structural core. Whereas $[\mathbf{1}]^{2+}$ and **3** are discrete diruthenium complexes, **2** has an extended structure in which the diruthenium units are bridged by $Ag(CN)_2^-$ and $Ag_2(CN)_3^-$ ions.

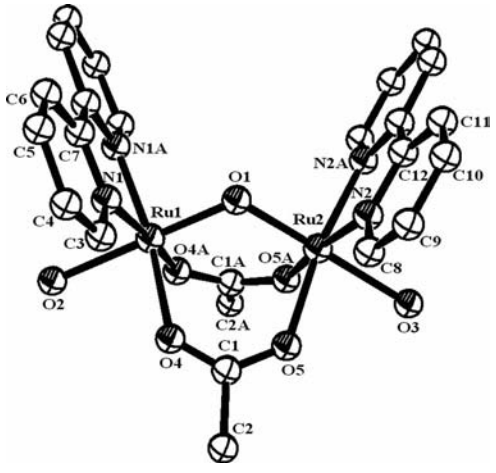


Figure 1. An ORTEP plot of $[\mathbf{1}]^{2+}$ with thermal ellipsoids at the 50% probability level. All hydrogen atoms and anions are omitted for clarity.

The complex cation $[\mathbf{1}]^{2+}$ (Figure 1) has a mirror plane that includes Ru1–O1–Ru2 as well as two oxygen atoms (O2 and O3) of the aqua ligands that are *trans* to the oxo bridge.

An asymmetric unit of polymeric **2** (Figure 2a) contains two $[Ru_2(\mu\text{-}O)(\mu\text{-}CH_3COO)_2(bpy)_2]^{2+}$ subunits in which the two *trans*-to-oxo sites are used for the bridging groups.

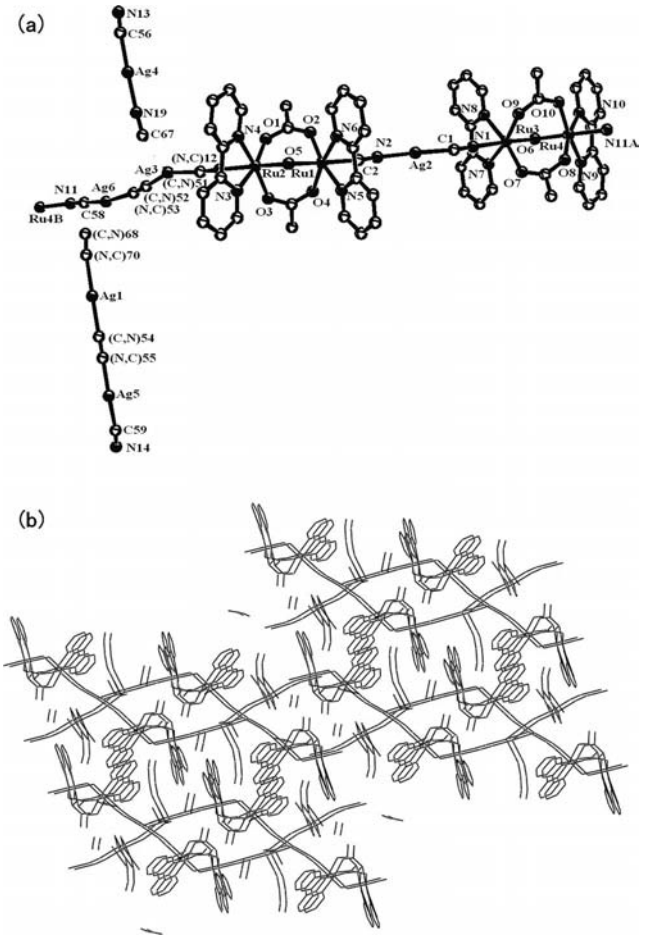


Figure 2. (a) An ORTEP plot of an asymmetric unit of **2** with thermal ellipsoids at the 50% probability level. All hydrogen atoms are omitted for clarity. (b) Packing structure of **2** in which the zigzag chains are connected through Ag···Ag interactions.

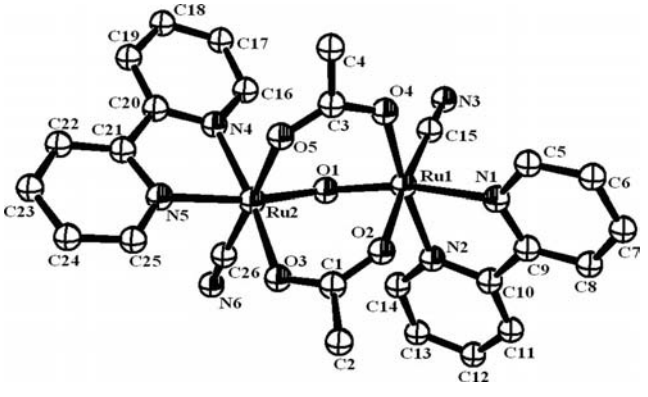


Figure 3. An ORTEP plot of **3** with thermal ellipsoids at the 50% probability level. All hydrogen atoms are omitted for clarity.

Thus the dimeric subunits are bridged by linear (CN)-$Ag(CN)^-$ or (CN)Ag(CN)$Ag(CN)^-$ ions by the coordination of either nitrogen or carbon atom of the cyano groups to the Ru centers at the *trans* positions of the μ-oxo ligand. The chain structure is expressed as NC–Ag6–XX–Ag3–XX–Ru2–O–Ru1–CN–Ag2–CN–Ru3–O–Ru4– for which

  

atomic numbering is as given in Figure 2a. The XX part consists of the crystallographically disordered C and N of one cyano ligand. The chain is significantly bent at the Ru–O–Ru part by the angle of around 122°, whereas the corresponding angles around Ag are in the range of 155–180°. The terminal cyano nitrogen of the chain coordinates to Ru4 of the next asymmetric unit to give a zigzag infinite cationic chain. Both of the ruthenium ions (Ru3 and Ru4) in one of the diruthenium subunit are coordinated by nitrogen atoms, whereas those of the other subunit (Ru1 and Ru2) are coordinated by one carbon and one disordered atom. The Ag–C (or N) distances in the chain range from 2.05 to 2.12 Å.

The asymmetric unit further contains one $Ag_2(CN)_3^-$ and one $Ag(CN)_2^-$ group. The carbon and nitrogen atoms of the two cyanides of this $Ag_2(CN)_3^-$ group are disordered and expressed as XX–Ag–XX–Ag–CN, whereas the $Ag(CN)_2^-$ group is expressed as NC–Ag–NC. These groups weakly interact with Ag6 [Ag6–X distance is 2.51(1) Å] and Ag3 [Ag3–C distance is 2.38(2) Å], respectively, of the $Ag_2(CN)_3^-$ group in the cationic chain. Since these distances are considerably longer than the Ag–N (or C) distances within the cationic chain, these additional $Ag_2(CN)_3^-$ and $Ag(CN)_2^-$ groups are regarded as counteranions rather than parts of the main framework of the complex.

One of the silver atoms (Ag3) of the $Ag_2(CN)_3^-$ group in the main chain forms weak Ag···Ag interactions (Ag–Ag distance 3.63 Å) with the silver atom of an $Ag(CN)_2^-$ group in another different chain, and the other silver atom Ag6 forms weak Ag···Ag interactions (the Ag–Ag distance 3.17 Å) with the counteranionic $Ag_2(CN)_3^-$ in a different chain. Thus, a three-dimensional network is formed through the weak Ag···Ag interactions (Figure 2b).

The geometrical structure of **3** (Figure 3) is an unexpected one, in that the cyano ligands occupy *cis*-to-oxo positions. Orientation of the bpy ligands in **3** is thus different from those of $[\mathbf{1}]^{2+}$ and **2**. In the case of **3**, the bpy ligand forms a chelate ring between *cis*-to-oxo and *trans*-to-oxo positions. Thus, the coordination sphere of each Ru is chiral. The overall structure of the dimer is also chiral, because the dimer has virtual twofold axis at the bridging oxygen atom. As shown by its space group $P\bar{1}$, the crystal of **3** is racemic and contains equal amounts of enantiomers. Each bridging acetate ion is *trans* to the cyano ligand of one Ru atom and to the nitrogen atom of the chelating bpy of another Ru atom. The μ-O–Ru–N(bpy) angles that involve a *trans*-to-oxo nitrogen are 168.8(2) and 167.8(2)°, and are significantly distorted from the ideal linear arrangement. The corresponding angles of $[\mathbf{1}]^{2+}$ [μ-O–Ru–O($H_2O$)] and **2** [μ-O–Ru–(C,N)(cyano)] are around 180 and 178°, respectively. The smaller angle of **3** is due to the significantly small N–Ru–N angle of bpy [77.7(2) and 77.3(2)° in **3**] that is sterically demanded by the chelate ring.

The structural parameters of the $Ru_2$(μ-O) cores of all the three complexes are almost identical. The Ru···Ru distances, the Ru–O(oxo) bond lengths, and the Ru–O(oxo)–Ru angles all fall in the relatively narrow range of 3.236–3.282 Å, 1.857–1.875 Å, and 121.21–122.08°, respectively. These parameters are also similar to those of the known complexes with this structural core.[4–9] Thus, the structure of the $Ru_2$(μ-O) core is not significantly affected by the type of ligands at *trans* to the oxo-bridge as well as those at *cis*-to-oxo sites. Also, it is interesting to note that the structure of the core is also insensitive to the significant distortion at the *trans*-to-oxo sites as observed for **3**.

The bond lengths at the *trans*-to-oxo sites are longer than those at the *cis*-to-oxo sites in all the complexes $[\mathbf{1}]^{2+}$, **2**, and **3** due to the *trans* influence of the μ-oxo ligand. Thus, the Ru–CN distances are significantly different between **2** and **3**. Whereas the distances are 1.971(5)–1.975(7) Å in **3**, in which $CN^-$ ligands are at *cis*-to-oxo sites, they are longer at 2.052(10)–2.111(11) Å in **2** with *trans*-to-oxo cyanide ligands.[12] The *trans*-to-oxo Ru–N bond lengths [2.094(5), 2.111(5) Å] of **3** are shorter than those [Ru–O($H_2O$) distances] of $[\mathbf{1}]^{2+}$. Again, the significant deviation of the *trans*-to-oxo nitrogen atoms from the ideal *trans* direction may be relevant. Nevertheless, they are still longer than the bond lengths of Ru–N(bpy) at *cis*-to-oxo sites [2.050(6), 2.060(5) Å].

The *trans* influence of the cyano ligand (*cis*-to-oxo) is clear in **3**. The bond lengths of Ru–O(acetate) *trans* to cyano ligands [2.153(3) and 2.148(5) Å for Ru1–O2 and Ru2–O5, respectively] are approximately 0.10 Å longer than those *cis* to cyano groups [2.040(5) and 2.049(4) Å for Ru1–O4 and Ru2–O3, respectively].

The different geometrical structures of **2** and **3** may be at least partially explained by considering the strong *trans* influence of the cyano ligand. The coordination of the cyano ligand at *trans*-to-oxo site would destabilize the dπ–pπ interaction of the Ru–O–Ru core. In the case of **2**, the *trans* influence from the cyano ligands would become weaker by the interaction of the other end of the ligand with $Ag^+$. The *cis*-to-oxo coordination of bare $CN^-$ in **3** would be the result of avoiding such destabilization of the Ru–O–Ru π system. This may be related to the fact that the phosphane complexes of the $Ru_2$(μ-O)(μ-RCOO)$_2$ core have phosphane ligands with appreciable π-bonding character at the *cis*-to-oxo sites in all the cases for which the X-ray structural analyses are available.[4g,4f,9a]

## Spectroscopic Properties

The IR spectra of $[\mathbf{1}]^{2+}$, **2**, and **3** in KBr pellets showed the bands of the acetate groups at around 1550 and 1420–1430 $cm^{-1}$. The former band corresponds to the asymmetric stretching mode [$\nu_{as}(COO^-)$], whereas the latter to the symmetric stretching [$\nu_s(COO^-)$]. The energy differences between the two bands [$\nu_{as}(COO^-)$–$\nu_s(COO^-)$] are 120–130 $cm^{-1}$, which falls in the range of values observed for bridging carboxylate ligands in inorganic metal compounds.[13] The IR spectrum of **2** showed three peaks at 2140, 2123, and 2102 $cm^{-1}$, which probably correspond to different types of $CN^-$ groups in the solid state. The $CN^-$ band of **3** is found in slightly lower energy at 2084 $cm^{-1}$.

  

The UV/Vis absorption spectra of the three complexes show strong bands in the 540–650 nm region. The discrete complexes $[\mathbf{1}][PF_6]_2{\cdot}H_2O$ and $[\mathbf{3}]{\cdot}CH_3OH{\cdot}H_2O$ are soluble in various solvents and exhibit a band at 566 and 558 nm, respectively, in $H_2O$ (Figure 4 and Table 1). The polymeric complex **2** is only slightly soluble in $CH_3CN$ and DMF. The polymeric structure **2** must be broken when dissolved into these solvents to give fragmented species. A mixture of fragmented species in solution is denoted as **2′**. ESI-MS spectra show some fragmented species that contain $Ru_2(\mu\text{-}O)(\mu\text{-}CH_3COO)_2$ cores {$[Ru_2(\mu\text{-}O)(\mu\text{-}CH_3COO)_2(bpy)_2(CN)_2]$, $[Ru_2(\mu\text{-}O)(\mu\text{-}CH_3COO)_2(bpy)_2(CN)_2\text{–}Ag]$, $[Ru_2(\mu\text{-}O)(\mu\text{-}CH_3COO)_2(bpy)_2(CN)_2\text{–}Ag\text{–}CN\text{–}Ag]$, and so forth} in $CH_3CN$. NMR spectroscopic signals of **2′** are too complicated to be assigned, thereby indicating that various fragmented species would contribute. Nevertheless, it is clear that the visible absorption band of **2′** appears at significantly lower energy region as a broad one centered at 636 nm. The spectrum of **2′** should represent various fragmented species with the common structural unit of *trans*(μ-O,CN)-$[Ru_2(\mu\text{-}O)(\mu\text{-}CH_3COO)_2(bpy)_2(CN)_2]$. Since no appreciable absorption is found in the region around 540–570 nm (which corresponds to the peak of **3**), migration of the $CN^-$ ligands to the *cis*-to-oxo positions is not significant, if it occurred, upon dissolution of **2**.

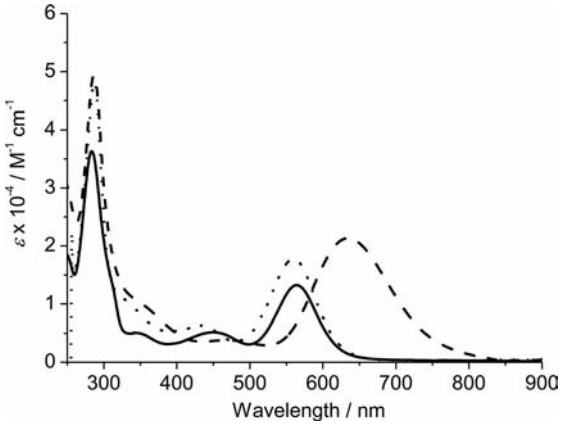


Figure 4. Electronic absorption spectra of $[\mathbf{1}]^{2+}$ (—, in $H_2O$), **2′** (-----, in $CH_3CN$), and **3** (·····, in $H_2O$).

The visible absorption band of $[\mathbf{1}]^{2+}$ shifts to longer wavelengths with the change of the solvent in the order: $H_2O < CH_3OH < C_2H_5OH < CH_3CN <$ DMF, with the largest shift being to 597 nm in DMF (Table 1). Since the aqua ligands of $[\mathbf{1}]^{2+}$ are readily replaced by solvent molecules, the species in solution must be $[Ru_2(\mu\text{-}O)(\mu\text{-}CH_3COO)_2(bpy)_2(S)_2]^{2+}$, in which S is a solvent molecule at *trans* positions to the oxo bridge. In fact, the independently prepared acetonitrile complex $[Ru_2(\mu\text{-}O)(\mu\text{-}CH_3COO)_2(bpy)_2(CH_3CN)_2]^{2+}$ ($[\mathbf{6}]^{2+}$)[11] shows the absorption peak at 587 nm, which is in excellent agreement with that of $[\mathbf{1}]^{2+}$ in $CH_3CN$. Recently, other aqua complexes of the $Ru_2(\mu\text{-}O)(\mu\text{-}CH_3COO)_2$ core, *trans*(μ-O,$H_2O$)-$[Ru_2(\mu\text{-}O)(\mu\text{-}CH_3COO)_2(py)_4(H_2O)_2]^{2+}$ and *trans*(μ-O,$H_2O$)-$[Ru_2(\mu\text{-}O)(\mu\text{-}CH_3COO)_2(4\text{-picoline})_4(H_2O)_2]^{2+}$, have been characterized in solution.[8] These complexes show a strong visible band at 559 and 556 nm, respectively, in acetone/water mixture.

Table 1. UV/Vis absorption spectroscopic data of complexes $[\mathbf{1}]^{2+}$, **2′**, and **3**.

| Complex | Solvent | $\lambda_{max}$ [nm] ($\varepsilon$ [$M^{-1}\,cm^{-1}$]) |
|---|---|---|
| $[\mathbf{1}]^{2+}$ | $H_2O$ | 284 (36000), 348 (5000), 450 (5000), 566 (12600) |
| | $CH_3OH$ | 287, 354, 457, 577 |
| | $CH_3CH_2OH$ | 254, 349, 462, 581 |
| | $CH_3COCH_3$ | 354, 468, 580 |
| | $CH_3CN$ | 242, 283, 345, 442, 587 |
| | DMF | 291, 355, 473, 597 |
| **2′** | $CH_3CN$ | 287 (49000), 352 (9400), 636 (21000) |
| | DMF | 289, 355, 477, 634 |
| **3** | $H_2O$ | 285 (48600), 330 (8100), 432 (6600), 558 (18000) |
| | $CH_3OH$ | 242 (38700), 288 (58700), 335 (11500), 435 (7000), 560 (22700) |
| | $CH_3CN$ | 289 (48000), 343 (10000), 454 (6200), 566 (21100) |
| | DMF | 293, 351, 458, 571 |
| | $CH_2C1_2$ | 249, 290, 342, 432, 561 |

The band maximum of **3** also depends on the type of solvents (Table 1). The band at 558 nm in aqueous solution shifts to the longer wavelength in $CH_3OH$ (560 nm), $CH_3CN$ (566 nm), and DMF (571 nm). In these cases, the substitution of the cyano ligands by the solvent molecules is highly unlikely within the time of measurements. The band shift is probably due to the formation of hydrogen bonds between the free end of the cyano ligands and the solvent molecules. The influence of metal ions on the band maximum of **3** was also investigated in $CH_3CN$ and water, since the cyano ligands in **3** may interact with metal ions at their free nitrogen end. It was found that the bands are blueshifted in $CH_3CN$ in the presence of $Ag^+$ (559 nm with 2.0 equiv. $AgNO_3$) or $Zn^{2+}$ [552 nm with 2.0 equiv. $Zn(ClO_4)_2$] (Figure 5). However, no band shift was observed in $H_2O$ or in $CH_3OH$ in the presence of the above-mentioned metal ions. The hydrogen bonds between the solvent molecules ($H_2O$ and $CH_3OH$) and the cyano groups are strong enough to prevent the interactions between the cyano groups and the metal ions. In the presence of $KAg(CN)_2$, the band shift is not observed even in $CH_3CN$. In this case, the coordination sphere of the $Ag^+$ is already saturated with free cyano groups and not available for the interaction with coordinated cyano groups.

To summarize the spectrophotometric results, it is interesting to note that although the transition energy of the band of **2′** (636 nm in $CH_3CN$) with *trans*-to-oxo $CN^-$ ligand is at the longest wavelength, that of **3** (558 nm in water) with *cis*-to-oxo $CN^-$ ligand is among the shorter wavelength observed so far for the complexes with the $Ru_2(\mu\text{-}O)(\mu\text{-}CH_3COO)_2$ core. The peak position of $[\mathbf{1}]^{2+}$ at 566 nm in water is also among the shortest band energies observed for the diruthenium complexes with aromatic amine ligands. Although the results show the important role of the *trans*-to-oxo ligand to the visible absorption

  

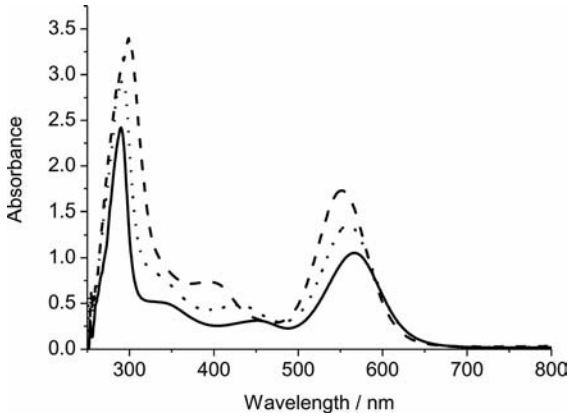


Figure 5. Electronic absorption spectra of **3** in $CH_3CN$ without additive (—) and with addition of two equivalents of $AgNO_3$ (·····) or $Zn(ClO_4)_2$ (-----) at the concentration of $5.0 \times 10^{-5}$ M.

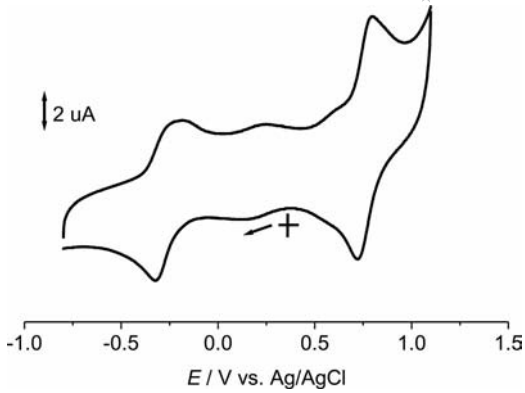


Figure 6. Cyclic voltammogram of $[\mathbf{1}]^{2+}$ (0.5 mM) in 0.1 M $NaClO_4$ aqueous solution. Scan rate: 50 mV s$^{-1}$.

band energies, it appears to be difficult to explain the results in terms of the simple dπ(Ru)–pπ(μ-O) orbital scheme. The electronic structure of these complexes will be discussed with the help of molecular orbital calculations in the latter part of this paper.

## Electrochemistry

The solvents employed for the measurements of cyclic voltammograms (CV) of the new complexes were limited due to ligand substitution for $[\mathbf{1}]^{2+}$ and low solubility for **2′** and **3**. As noted above, $[\mathbf{1}]^{2+}$ in nonaqueous solvents undergoes substitution reactions of solvent molecules for the aqua ligands. The CV of $[\mathbf{1}]^{2+}$ in 0.1 M $NaClO_4$ aqueous solution (pH = 6.59) (Figure 6) shows two distinct redox couples at $E_{1/2}$ = –0.31 and +0.76 V versus Ag/AgCl, which are assigned to the $Ru_2^{II,III}/Ru_2^{III,III}$ and $Ru_2^{III,III}/Ru_2^{III,IV}$ processes, respectively. The redox couples shift to positive potential region in 0.1 M $HClO_4$ solution, in which three one-electron redox waves were observed at –0.15, –0.03, and +0.83 V. The most negative wave can be assigned to the $Ru_2^{II,II}/Ru_2^{II,III}$ process. The pH dependence must be due to the protonation at the oxo bridge in acid solution and the deprotonation of the aqua ligand(s) in solutions of higher pH. The pH dependence of the redox potentials are thus complicated, and further details of the proton-coupled redox behavior of $[\mathbf{1}]^{2+}$ that are under investigation will be reported separately.

It was difficult to obtain a clear cyclic voltammogram of **2′** in acetonitrile due to low solubility in the presence of the electrolytes. Nevertheless, a weak redox wave was found in 0.1 M $n$Bu$_4$NPF$_6$ acetonitrile at around $E_{1/2}$ = –0.77 V versus Ag/AgCl that may correspond to the $Ru_2^{II,III}/Ru_2^{III,III}$ process. Although complex **3** was also slightly soluble in most solvents with electrolytes, the two redox potentials were observed in 0.1 M $n$Bu$_4$NPF$_6$/DMF and 0.1 M $n$Bu$_4$NPF$_6$/$CH_2Cl_2$ solutions at $E_{pc}$ = –0.71 V and $E_{1/2}$ = +0.82 V and at $E_{pc}$ = –0.83 V and $E_{1/2}$ = +0.76 V versus Ag/AgCl, respectively. In the former solvent, the free nitrogen end of the cyano ligands would interact with the solvent molecule and the Ru–N bond may be weakened, whereas it is unlikely that $CH_2Cl_2$ interacts similarly.

The redox potentials of **2′** and **3** were found in more negative potential regions than those of the $Ru_2$(μ-O)(μ-$CH_3COO)_2$ complexes with only N-heterocyclic ligands (–0.30 to –0.60 V and +0.76 to +0.96 V for the $Ru_2^{II,III}/Ru_2^{III,III}$ and $Ru_2^{III,III}/Ru_2^{III,IV}$ processes, respectively).[6e] The significantly negative potential shift of the redox potentials of the $Ru_2^{II,III}/Ru_2^{III,III}$ process is particularly noted. This is probably due to the strong electron donation of the $CN^-$ ligands. Details will be discussed in the next section with the aid of molecular orbital calculations.

## Theoretical Investigations on the Energy Levels of the Molecular Orbitals

Before discussing the details of the theoretical calculations, it may be worth mentioning a general view of the electronic structures of the $Ru_2$(μ-O)(μ-$OOCCH_3)_2$ core.[5] The qualitative molecular orbital scheme of the core that is based on the dπ(Ru)–pπ(μ-O) interaction is shown in Figure 7, in which the *x*, *y*, and *z* axes of the Ru atom are also depicted. The strongest dπ–pπ interaction involves the Ru $d_{zx}$ and μ-O $\pi_x$ orbitals that are perpendicular to the $Ru_2$(μ-O) plane and gives one bonding ($\pi_1$), one nonbonding ($n_2$), and one antibonding orbital ($\pi_2$*). The interaction that involves $d_{yz}$ orbitals is less significant ($\pi_2$, $n_1$, and $\pi_1$*), and that with $d_{xy}$ orbitals is even weaker (essentially nonbonding orbitals). The nonbonding orbitals ($n_1$ and $d_{xy}$ components) stay around that of the nonbonding orbital of the $d_{zx}$–$\pi_x$ interaction ($n_2$) in energy. Since the trivalent Ru has five d electrons, all the orbitals except for $\pi_2$* are occupied. Under this molecular orbital scheme (Figure 7), the strong visible absorption band has been assigned to either an $\pi_1 \rightarrow \pi_2$* or $n_2 \rightarrow \pi_2$* transition.[5] As will be noted later, however, observed electronic transition energies of the new cyano complexes are not fully explained by this simple molecular orbital scheme.

  

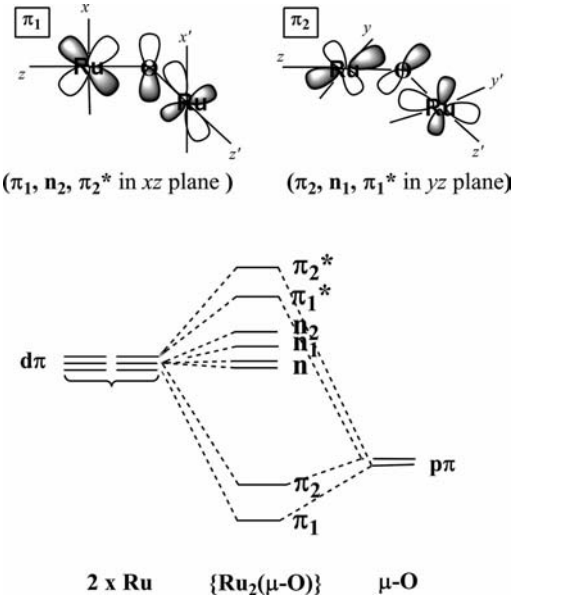


Figure 7. Qualitative molecular orbital scheme for the Ru(dπ)–μ-O(pπ) interaction of the bent Ru–O–Ru moiety.

To obtain further insight into the electronic structures and spectroscopic properties of these complexes, we carried out molecular orbital (MO) calculations on complexes $[\mathbf{1}]^{2+}$, $[Ru_2(\mu\text{-}O)(\mu\text{-}OOCCH_3)_2(bpy)_2(CN)_2]$ (**2a**) (a model compound of **2′**, $CN^-$ is carbon bonded and *trans* to the oxo ligand), **3** ($CN^-$ is carbon bonded and *cis* to the oxo ligand), $[Ru_2(\mu\text{-}O)(\mu\text{-}OOCCH_3)_2(py)_6]^{2+}$ ($[\mathbf{4}]^{2+}$), and $[Ru_2(\mu\text{-}O)(\mu\text{-}OOCCH_3)_2(bpy)_2(py)_2]^{2+}$ ($[\mathbf{5}]^{2+}$) (py is *trans* to the oxo ligand) by using the density functional theory (DFT) method.

The calculations for the ground-state molecular structures revealed the energy levels and the components of the MOs near the frontier orbitals as listed in Table 2. The highest-occupied MO (HOMO) and the lowest-unoccupied MO (LUMO) in all the cases are mainly composed of ruthenium and bridging oxo orbitals, in which the Ru d orbitals mix well with the oxo p orbitals. Whereas the contribution of Ru d orbitals to HOMO and LUMO is in the range of 50–70%, that from p orbitals of the bridging oxo ligand is also significant by around 35 and 20% for LUMO and HOMO, respectively. Thus, earlier qualitative descriptions based on the dπ(Ru)–pπ(μ-O) interaction (Figure 7) are principally supported. The $\pi_2$* orbital is approximated to LUMO, and the $\pi_1$* orbital to HOMO. The $\pi_2$, $n_1$, $n_2$, and other n orbitals may correspond to one of the orbitals of the nearby HOMO region (HOMO–1, HOMO–2, HOMO–3, HOMO–4, and so on), and the bonding orbital $\pi_1$ is in the deep bonding orbital region.

Energies of LUMO, HOMO, and some bonding orbitals (e.g., HOMO–1, HOMO–2, HOMO–3, HOMO–4) are affected by the ligands around the $Ru_2(\mu\text{-}O)$ core. Contributions of the bridging acetates to LUMO and HOMO are generally small, but those to HOMO–1, HOMO–2, HOMO–3, and HOMO–4 are often close to 10–20%. The *cis*-to-oxo ligands, bpy or *cis*-py, contribute to these orbitals by at most 18%. Contributions of the ligands *trans* to the oxo bridge are not as significant as we initially expected. Whereas the contributions from pyridine ($[\mathbf{4}]^{2+}$ and $[\mathbf{5}]^{2+}$) and aqua ligands ($[\mathbf{1}]^{2+}$) are less than 6%, that from cyano ligands in **2a** is relatively large for HOMO, HOMO–1, and HOMO–2 (13–18%). It is noted that HOMO and HOMO–2 of **2a** are approximated to the components of the in-plane Ru(dπ)–O(pπ) interaction ($\pi_2$, $n_1$, and $\pi_1$* in Figure 7), whereas HOMO–1 is approximated to the out-of-plane Ru(dπ)–O(pπ) one ($n_2$). It may be interesting to compare these results with those of **3**, in which higher con-

Table 2. Composition of the frontier orbitals for $[\mathbf{1}]^{2+}$, **2a**, **3**, $[\mathbf{4}]^{2+}$, and $[\mathbf{5}]^{2+}$.

| | MO | MO energy [eV] | Component [%] Ru | μ-O | aqua | acetate | bpy |
|---|---|---|---|---|---|---|---|
| $[\mathbf{1}]^{2+}$ | LUMO+1 | –7.69 | 4 | 0 | 0 | 0 | 95 |
| | LUMO | –8.95 | 58 | 35 | 1 | 2 | 5 |
| | HOMO | –11.04 | 61 | 21 | 4 | 2 | 11 |
| | HOMO–1 | –11.33 | 71 | 1 | 1 | 20 | 7 |
| | HOMO–2 | –11.35 | 78 | 0 | 1 | 8 | 13 |
| | HOMO–3 | –11.48 | 78 | 0 | 2 | 10 | 9 |
| | HOMO–4 | –12.12 | 88 | 0 | 0 | 9 | 3 |

| | | | Component [%] Ru | μ-O | $CN^-$ | acetate | bpy |
|---|---|---|---|---|---|---|---|
| **2a** | LUMO+2 | –2.57 | 6 | 2 | 1 | 0 | 92 |
| | LUMO+1 | –2.59 | 5 | 0 | 0 | 0 | 94 |
| | LUMO | –3.26 | 50 | 35 | 6 | 2 | 7 |
| | HOMO | –5.08 | 47 | 24 | 13 | 1 | 15 |
| | HOMO–1 | –5.47 | 69 | 0 | 17 | 8 | 7 |
| | HOMO–2 | –5.56 | 60 | 4 | 18 | 11 | 8 |
| | HOMO–3 | –5.84 | 71 | 0 | 3 | 22 | 3 |
| | HOMO–4 | –6.37 | 87 | 0 | 1 | 9 | 4 |

| | | | Component [%] Ru | μ-O | $CN^-$ | acetate | bpy |
|---|---|---|---|---|---|---|---|
| **3** | LUMO+2 | –2.21 | 7 | 2 | 7 | 1 | 83 |
| | LUMO+1 | –2.27 | 4 | 0 | 5 | 1 | 90 |
| | LUMO | –2.96 | 54 | 33 | 1 | 3 | 9 |
| | HOMO | –5.04 | 60 | 18 | 8 | 3 | 11 |
| | HOMO–1 | –5.16 | 65 | 2 | 10 | 14 | 10 |
| | HOMO–2 | –5.35 | 67 | 1 | 10 | 7 | 16 |
| | HOMO–3 | –5.47 | 81 | 3 | 3 | 9 | 4 |
| | HOMO–4 | –5.65 | 61 | 0 | 15 | 6 | 18 |

| | | | Component [%] Ru | μ-O | *trans*-py | acetate | *cis*-py |
|---|---|---|---|---|---|---|---|
| $[\mathbf{4}]^{2+}$ | LUMO+1 | –6.61 | 2 | 0 | 1 | 0 | 97 |
| | LUMO | –8.48 | 55 | 32 | 5 | 3 | 5 |
| | HOMO | –10.51 | 65 | 20 | 5 | 4 | 6 |
| | HOMO–1 | –10.79 | 75 | 2 | 3 | 12 | 7 |
| | HOMO–2 | –10.82 | 77 | 1 | 5 | 9 | 9 |
| | HOMO–3 | –10.90 | 76 | 1 | 1 | 14 | 9 |
| | HOMO–4 | –11.34 | 82 | 0 | 1 | 8 | 9 |

| | | | Component [%] Ru | μ-O | py | acetate | bpy |
|---|---|---|---|---|---|---|---|
| $[\mathbf{5}]^{2+}$ | LUMO+2 | –7.20 | 3 | 0 | 0 | 0 | 97 |
| | LUMO+1 | –7.23 | 4 | 0 | 1 | 0 | 95 |
| | LUMO | –8.34 | 54 | 34 | 6 | 2 | 4 |
| | HOMO | –10.43 | 60 | 24 | 3 | 2 | 11 |
| | HOMO–1 | –10.7 | 77 | 0 | 6 | 8 | 9 |
| | HOMO–2 | –10.82 | 71 | 1 | 1 | 22 | 5 |
| | HOMO–3 | –10.97 | 77 | 1 | 2 | 10 | 10 |
| | HOMO–4 | –11.5 | 87 | 0 | 0 | 9 | 3 |

  

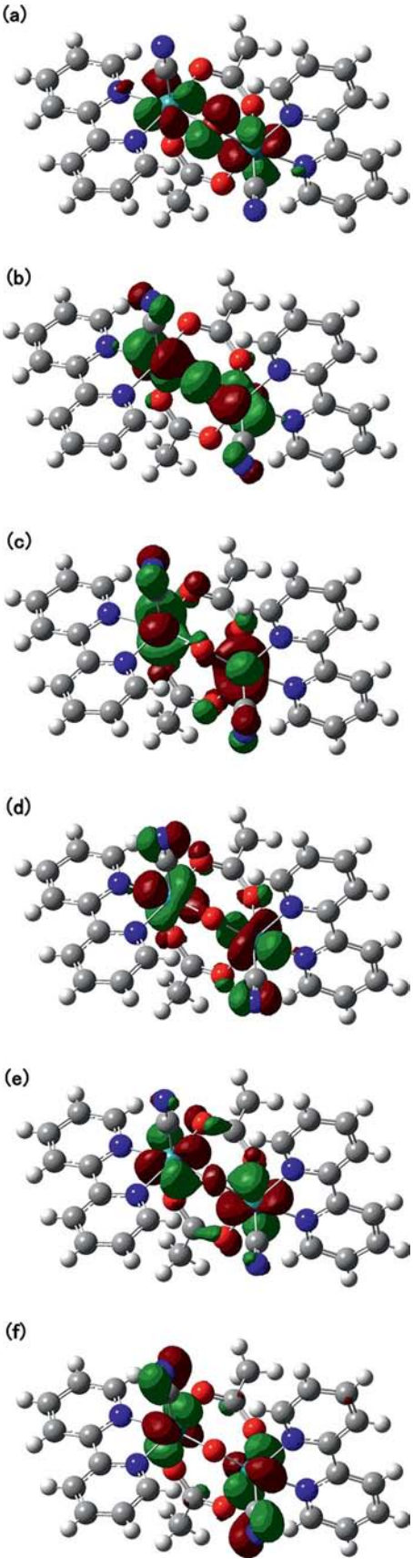


Figure 8. Contour plots of molecular orbitals of **3**: (a) LUMO, (b) HOMO, (c) HOMO–1, (d) HOMO–2, (e) HOMO–3, and (f) HOMO–4.

tribution of the *cis*-to-oxo cyano ligand (>10%) is seen in the orbitals that are essentially in $d_{xy}$ (HOMO–1 and HOMO–4) and $d_{yz}$ origins (HOMO–2). Clearly, the cyano ligands in **3** contribute by the lesser extent to the Ru–O–Ru dπ–pπ interaction.

Energies of these frontier orbitals (LUMO+1, LUMO, HOMO, HOMO–1, HOMO–2, HOMO–3, and HOMO–4) are generally higher for the two cyano complexes than the other three complexes. The two negatively charged cyano ligands make the overall charge of the complexes neutral and would cause the shift of the energy levels under discussion to somewhat higher including LUMO+1, which is almost purely localized on the bpy ligands. If the energy difference between the LUMO+1 and LUMO (primarily Ru d character) is compared between $[\mathbf{1}]^{2+}$, **2a**, **3**, and $[\mathbf{5}]^{2+}$, it is still considerably smaller for the two cyano complexes. Thus the further increase in the energy levels of Ru d orbitals is obvious, which would be due to stronger π-donor ability of the $CN^-$ ligands. Cyanide anion generally acts as ligand-to-metal σ donor as well as metal-to-ligand π acceptor. In the present cases, however, the cyano ligands act as a π donor as indicated by the components (Tables S4 and S5 in the Supporting Information) and the contour plots of MOs (Figure 8).[14] It is concluded that the $Ru_2(\mu\text{-}O)(\mu\text{-}CH_3COO)_2$ core is a poor π donor and acts as π acceptor toward the $CN^-$ ligands in spite of the $d^5$ electronic configuration.

### Theoretical Investigations on the Electronic Transitions

Transition energies and oscillator strengths of the lowest ten spin-allowed transitions around the HOMO–LUMO region were calculated for each of the five complexes $[\mathbf{1}]^{2+}$, **2a**, **3**, $[\mathbf{4}]^{2+}$, and $[\mathbf{5}]^{2+}$ (the results are listed in Tables S6–S10, respectively, in the Supporting Information). It should be noted that the HOMO–LUMO transitions are symmetry-forbidden for all the complexes. Whereas LUMO is oriented perpendicularly to the Ru–O–Ru plane, HOMO is within the plane (see Figure 8). The symmetrically allowed lowest-energy transitions were evaluated to understand the origin of the strong visible absorption band. The lowest-energy transition thus found is the combination of several components (Figure 9). The calculated main transitions of all the five complexes are listed in Table 3. The calculated spectra of the five complexes are shown in Figures S1–S4, which are in good agreement with the observed spectra.

For $[\mathbf{1}]^{2+}$, $[\mathbf{4}]^{2+}$, and $[\mathbf{5}]^{2+}$, the largest contribution to the substantially allowed lowest-energy transition is that from HOMO–2, HOMO–2, and HOMO–1 to LUMO, respectively. The transitions correspond to an $n_2 \rightarrow \pi_2^*$ transition in the qualitative MO scheme in Figure 7, and may be considered metal-to-metal charge transfer (MMCT) type.

On the contrary, the major component of the transition of **2a** is from HOMO ($\pi_1^*$) to LUMO+1 (approximated to π* orbitals of bpy ligands). Thus, the transition corresponds to the metal-to-ligand charge-transfer (MLCT) type. The lowest-energy transition of **3** is the combination

  

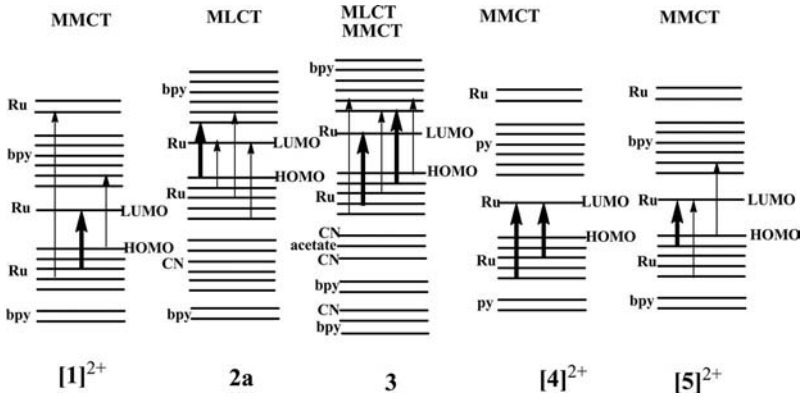


Figure 9. Allowed lowest excited states of $[\mathbf{1}]^{2+}$, **2a**, **3**, $[\mathbf{4}]^{2+}$, and $[\mathbf{5}]^{2+}$. Thick arrows indicate major transitions, and thin ones minor transitions. The element symbol on the left side of each orbital indicates its main component. The sequence of the energy levels of molecular orbitals is depicted qualitatively but not quantitatively.

Table 3. Substantially allowed lowest-energy transitions for $[\mathbf{1}]^{2+}$, **2a**, **3**, $[\mathbf{4}]^{2+}$, and $[\mathbf{5}]^{2+}$.

| Complex | Energy [eV] ($\lambda$ [nm]) | Oscillator strength | Major contribution | Percentage [%] | Assignment |
|---|---|---|---|---|---|
| $[\mathbf{1}]^{2+}$ | 2.134 (581) | 0.1623 | HOMO–2 → LUMO | 58 | MMCT |
| **2a** | 1.877 (661) | 0.1748 | HOMO → LUMO+1 | 72 | MLCT |
| | | | HOMO–1 → LUMO | 9 | MMCT |
| **3** | 2.160 (574) | 0.2502 | HOMO–3 → LUMO | 41 | MMCT |
| | | | HOMO–1→ LUMO+1 | 17 | MLCT |
| $[\mathbf{4}]^{2+}$ | 2.197 (564) | 0.1815 | HOMO–4 → LUMO | 24 | MMCT |
| | | | HOMO–2 → LUMO | 36 | MMCT |
| $[\mathbf{5}]^{2+}$ | 2.116 (586) | 0.2641 | HOMO–1 → LUMO | 54 | MMCT |

of MMCT and MLCT. The different characteristics of the transitions of these cyano complexes are the consequence of the narrower energy gap between the occupied orbitals of essentially Ru d origin and the 2,2′-bpy π* orbitals (vide supra). In these cases, MLCT transition energies become comparable to or smaller than those of MMCT transitions.

Despite similar energy levels of HOMO and bpy π* orbitals, the energies of the lowest allowed transitions are significantly different between **2a** and **3**. The difference is ascribed to the different occupied orbitals from which the transition to bpy π* orbitals takes place. Closer investigation of MOs revealed that the different orientation of bpy toward the HOMO is important for the transitions. Whereas the lower-energy transition from HOMO to π* (bpy) is a major component for **2a**, the corresponding transition is practically forbidden and the higher-energy transition from the lower occupied orbital becomes more important for **3**. In the latter case, the transition energy of MLCT becomes comparable to that of the MMCT transition ($n_2 \rightarrow \pi_2^*$).

For the MMCT transitions of $[\mathbf{1}]^{2+}$, $[\mathbf{4}]^{2+}$, and $[\mathbf{5}]^{2+}$, the occupied orbitals that have a similar distribution to LUMO are primarily responsible for the allowed transition to LUMO (which corresponds to $n_2 \rightarrow \pi_2^*$ as mentioned above). This transition is HOMO–1 → LUMO for $[\mathbf{5}]^{2+}$ and HOMO–2 → LUMO for $[\mathbf{1}]^{2+}$ and $[\mathbf{4}]^{2+}$. The substantially higher transition energy of the aqua complex $[\mathbf{1}]^{2+}$ is noted, which might be explained by the weaker electron-donating ability of the aqua ligand that influences the dπ(Ru)–pπ(μ-O) interaction to a much lesser extent and leaves energy separation between $n_2$ and $\pi_2^*$ higher.

## Conclusion

The electronic structure of oxo-bis(acetato)-bridged diruthenium complexes was previously understand in terms of the qualitative dπ(Ru)–pπ(μ-O) interaction scheme. In this study, cyano ligands have been introduced as strongly influential nonbridging ligands to the dinuclear core, $Ru_2(\mu\text{-}O)(\mu\text{-}CH_3COO)_2(bpy)_2$, to find further details of the electronic structure of the diruthenium core. The two new geometrically isomeric cyano complexes of the general formula, $[Ru_2(\mu\text{-}O)(\mu\text{-}CH_3COO)_2(bpy)_2(CN)_2]$ [**3** *cis*(μ-O,CN)] and partial structure of the extended solid of **2** [*trans*(μ-O,CN)], and the newly isolated aqua complex *trans*(μ-O,$H_2O$)-$[Ru_2(\mu\text{-}O)(\mu\text{-}CH_3COO)_2(bpy)_2(H_2O)_2]^{2+}$ ($[\mathbf{1}]^{2+}$) have provided important information about the stereochemistry (distortion around the dinuclear core) and redox and spectrophotometric properties of this type of diruthenium complexes. The strong visible absorption bands that characterizes the electronic state of the $[Ru_2(\mu\text{-}O)(\mu\text{-}CH_3COO)_2]$ complexes appear at 558 and 636 nm for the *cis*(μ-O,CN) (in water) and *trans*(μ-O,CN) (in acetonitrile) complexes, respectively, which are among the longest and the shortest wavelengths for this type of complex. These properties have

  

been successfully explained with the help of the MO calculations of these and related complexes {$[Ru_2(\mu\text{-}O)(\mu\text{-}CH_3COO)_2(py)_6]^{2+}$ ($[\mathbf{4}]^{2+}$) and *trans*[μ-O,N(py)]-$[Ru_2(\mu\text{-}O)(\mu\text{-}CH_3COO)_2(bpy)_2(py)_2]^{2+}$ ($[\mathbf{5}]^{2+}$)}.

The calculations verified the involvement of the MLCT transitions to bpy π* orbitals in addition to the transitions within the core based on the dπ(Ru)–pπ(μ-O) interaction. Whereas the transitions for $[\mathbf{1}]^{2+}$ (566 nm in water), $[\mathbf{4}]^{2+}$ (587 nm in acetonitrile), and $[\mathbf{5}]^{2+}$ (599 nm in acetonitrile) are ascribed to n → π* transitions within the dπ(Ru)–pπ(μ-O) molecular orbital scheme perpendicular to the Ru–O–Ru plane, and are thus of MMCT type, those of the two cyano complexes are significantly different due to the increase in the energy of the metal dπ orbitals by the coordination of the cyano ligands. This makes the MLCT transition energies to the bpy π* orbitals lower than (in the case of **2a**) or comparable to the MMCT transition energies (for **3**). Thus, the transition is practically of almost pure MLCT type for **2a** and a mixture of MMCT and MLCT for **3**. Here the importance of different sites of the cyano coordination is also verified.

## Experimental Section

**General:** Reagents and solvents used were of commercially available reagent-grade quality unless otherwise stated. Acetonitrile used for the electrochemical measurements was distilled from $CaH_2$ under an Ar atmosphere. A diruthenium complex, *trans*(μ-O,$CH_3CN$)-$[Ru_2(\mu\text{-}O)(\mu\text{-}CH_3COO)_2(bpy)_2(CH_3CN)_2][PF_6]_2$, which was used for the preparation of the cyano complexes, was prepared as described previously.[11] The column chromatography for the purification of the complexes was performed by using silica gel (Wakogel C-300HG).

**Complex $[\mathbf{1}][PF_6]_2\cdot H_2O$:** $RuCl_3\cdot nH_2O$ (0.48 g, 2.30 mmol) was added to a mixed solvent of water (40 $cm^3$), acetic acid (30 $cm^3$), and ethanol (16 $cm^3$), and the solution was kept at 70 °C for 10 min. After the addition of a solution of bpy (0.80 g, 5.12 mmol) in ethanol (5 $cm^3$), the mixture was kept at 90 °C for 15 min. The solution was then cooled to room temperature, and an aqueous solution (40 $cm^3$) of $NH_4PF_6$ (4.0 g, 24.6 mmol) was added. The resulting dark brown solution was stored in a refrigerator (–5 °C) for 24 h. The solution was then filtered to collect the deposited solid, which was washed with small amount of water. The filtrate and the washings were discarded. Further washing of the solid in the frit with water to dissolve the solid gave a purple solution. The purple solution was evaporated to dryness to obtain a purple solid of $[\mathbf{1}][PF_6]_2\cdot H_2O$; yield 0.73 g (65%). $C_{24}H_{28}F_{12}N_4O_8P_2Ru_2$ (992.58): calcd. C 29.04, H 2.84, N 5.64; found C 28.96, H 3.04, N 5.80. ESI-MS (positive, in $H_2O$): *m*/*z* = 829.97 $[M - PF_6]^+$, 683.99 $[M - 2PF_6 + H]^+$, 668.98 $[M - 2PF_6 - H_2O + H]^+$, 343.01 $[M - 2PF_6]^{2+}$, 334.00 $[M - 2PF_6 - H_2O]^{2+}$, 323.99 $[M - 2PF_6 - 2H_2O]^{2+}$. IR (KBr): $\tilde{\nu}$ = 1553 [$\nu_{as}(COO^-)$], 1429 [$\nu_s(COO^-)$], 844 ($PF_6^-$) $cm^{-1}$. $^1H$ NMR ($D_2O$): $\delta$ = 2.21 (s, 6 H, $CH_3COO^-$), 6.14 (d, 4 H, 6,6′-H of bpy), 7.22 (t, 4 H, 5,5′-H of bpy), 7.96 (t, 4 H, 4,4′-H of bpy), 8.57 (d, 4 H, 3,3′-H of bpy) ppm. Single crystals of $[\mathbf{1}][PF_6]_2\cdot 3H_2O$ for the X-ray structural analysis were obtained from the initial purple solution on standing.

**Complex 2:** $KAg(CN)_2$ (19.5 mg, 0.098 mmol) was added to an aqueous solution (10 $cm^3$) of $[Ru_2(\mu\text{-}O)(\mu\text{-}OOCCH_3)_2(bpy)_2(CH_3CN)_2][PF_6]_2$[11] (100 mg, 0.098 mmol). The solution was stirred at room temperature for 4 h, during which time a blue precipitate appeared. The precipitate was filtered and washed with water (10 $cm^3$). Acetonitrile (50 $cm^3$) was added to the precipitate, and the resulting suspension was kept at 65 °C for 5 min to obtain maximum dissolution of the solid. After filtration, dichloromethane (5 $cm^3$) was added to the filtrate. The resulting solution was stored at –5 °C. Single crystals of **2** were obtained after one week. The crystals were collected and dried in vacuo; yield 0.015 g (13%). $C_{67}H_{58}Ag_6Cl_2N_{22}O_{10}Ru_4$ (2453.73): calcd. C 32.80, H 2.38, N 12.56; found C 32.29, H 2.51, N 12.05. ESI-MS (positive, in MeCN): *m*/*z* = 702.9 $[Ru_2(\mu\text{-}O)(\mu\text{-}CH_3COO)_2(bpy)_2(CN)_2 + H]^+$, 808.8 $[Ru_2(\mu\text{-}O)(\mu\text{-}CH_3COO)_2(bpy)_2(CN)_2\text{–}Ag]^+$, 942.7 $[Ru_2(\mu\text{-}O)(\mu\text{-}CH_3COO)_2(bpy)_2(CN)_2\text{–}Ag\text{–}CN\text{–}Ag]^+$, and so forth. IR (KBr): $\tilde{\nu}$ = 2140 ($CN^-$), 2123 ($CN^-$), 2102 ($CN^-$), 1548 [$\nu_{as}(COO^-)$], 1420 [$\nu_s(COO^-)$] $cm^{-1}$.

**Complex $[\mathbf{3}]\cdot CH_3OH\cdot H_2O$:** The initial blue precipitate obtained during the preparation of **2** was also used for the preparation of **3**. The blue precipitate was suspended in acetonitrile (100 $cm^3$), to which an aqueous solution (10 $cm^3$) of NaCl (30 mg, 0.51 mmol) was added. The suspension was then kept at 70 °C for 30 min, during which time the solid was partially dissolved by the reaction with NaCl. The remaining solid was removed by filtration. The filtrate was evaporated under reduced pressure to leave a blue purple solid. The solid was dissolved in acetonitrile (5 $cm^3$), and the solution was subjected to the chromatography on a silica gel column (Wakogel C-300HG). A purple species (second fraction) was separated by elution with methanol and the solvent was evaporated to obtain dark purple solid of $[\mathbf{3}]\cdot CH_3OH\cdot H_2O$; yield 0.025 g (36%). Single crystals for X-ray analysis were grown from a $CH_3OH$ solution at room temperature. $C_{27}H_{28}N_6O_7Ru_2$ (750.70): calcd. C 43.20, H 3.76, N 11.19; found C 43.46, H 3.84, N 11.27. ESI-MS (positive, in $CH_3OH$): *m*/*z* = 723.9 $[M + Na]^+$. IR (KBr): $\tilde{\nu}$ = 2084 ($CN^-$), 1545 [$\nu_{as}(COO^-)$], 1412 [$\nu_s(COO^-)$] $cm^{-1}$. $^1H$ NMR ($CD_3OD$): $\delta$ = 9.67 (d, 2 H), 9.09 (d, 2 H), 8.62 (d, 2 H), 8.39 (t, 2 H), 8.38 (t, 2 H), 8.20 (t, 2 H), 8.08 (*t*, 2 H), 7.42 (t, 2 H) ppm.

**Physical Measurements:** Ultraviolet and visible absorption spectra were measured with a JASCO V-560 spectrophotometer. $^1H$ NMR spectra were obtained with an EXC-400 NMR spectrometer at 400 MHz. Infrared absorption spectra were recorded with a Bio-Rad FTS 60A/896 FTIR spectrometer. Electrochemical measurements were carried out at room temperature with a potentiostat (EG&G, Model 263A) with a glassy-carbon working electrode. The potentials were recorded versus Ag/AgCl (saturated KCl solution) electrode. A Pt mesh was used as the counter electrode. Cyclic voltammetry was carried out for $[\mathbf{1}]^{2+}$ in 0.1 M $NaClO_4$ (pH = 6.59) and 0.1 M $HClO_4$ (pH = 1.53) aqueous solutions, for **2′** in 0.1 M $nBu_4NPF_6$ acetonitrile solution, and for **3** in solutions of 0.1 M $nBu_4NPF_6$ in DMF and 0.1 M $nBu_4NPF_6$ in $CH_2Cl_2$. Mass spectrometry and elementary microanalyses were performed at the Center for Instrumental Analysis, Hokkaido University.

**Crystal Structure Determination:** A single crystal of each of the three complexes was mounted on a glass fiber. Measurements were made on a Mercury CCD area detector coupled with a Rigaku AFC-8S diffractometer with graphite-monochromated Mo-$K_\alpha$ radiation. Final cell parameters were obtained from a least-squares analysis of reflections with $I > 10\sigma(I)$. Space-group determinations were made on the basis of systematic absences, a statistical analysis of intensity distribution, and the successful solution as well as refinement of the structures. Data were collected at a temperature of –120 °C to a maximum $2\theta$ value of 55°. Data were processed with Crystal Clear.[15] An empirical absorption correction resulted in acceptable transmission factors. The data were corrected for Lorentz

  

Table 4. Crystallographic data for complexes [**1**][$PF_6$]$_2$·3$H_2O$, [**2**], and [**3**]·$CH_3OH$·$H_2O$.

| | [**1**][$PF_6$]$_2$·3$H_2O$ | [**2**] | [**3**]·$CH_3OH$·$H_2O$ |
|---|---|---|---|
| Formula | $C_{24}H_{26}N_4O_7F_{12}P_2Ru_2$·3$H_2O$ | $C_{67}H_{58}N_{22}O_{10}Ru_4Ag_6Cl_2$ | $C_{26}H_{22}N_6O_5Ru_2$·$CH_3OH$·$H_2O$ |
| $M_r$ | 1028.61 | 2453.73 | 750.70 |
| Crystal system | monoclinic | triclinic | triclinic |
| Space group | *C*2/*m* | $P\bar{1}$ | $P\bar{1}$ |
| *a* [Å] | 15.570(3) | 11.751(5) | 8.348(2) |
| *b* [Å] | 18.944(4) | 14.433(6) | 9.380(3) |
| *c* [Å] | 14.752(3) | 26.034(12) | 19.978(6) |
| *α* [°] | – | 85.47(2) | 89.436(10) |
| *β* [°] | 119.5912(10) | 89.89(2) | 78.602(7) |
| *γ* [°] | – | 67.408(12) | 69.174(7) |
| *V* [Å$^3$] | 3783.9(13) | 4062.0(29) | 1430.2(7) |
| *Z* | 4 | 2 | 2 |
| Reflns. measd. $2° < 2\theta < 55°$ | 15203 | 21974 | 9655 |
| Number of variables | 260 | 1001 | 380 |
| $R$[a] | 0.054 | 0.101 | 0.052 |
| $wR$[b] | 0.156 | 0.235 | 0.119 |
| GOF | 1.098 | 1.199 | 1.076 |

[a] $R = \Sigma||F_o| - |F_c||/\Sigma|F_o|$. [b] $wR = \{\Sigma[w(F_o^2 - F_c^2)^2]/\Sigma[w(F_o^2)^2]\}^{1/2}$ with $w = (\sigma^2[F_o^2] + \{x[\max(F_o^2,0) + 2F_c^2]/3\}^2)^{-1}$.

and polarization factors. All calculations were performed with the CrystalStructure[16] crystallographic software package except for refinement, which was carried out with SHELXL-97.[17] The structures were solved by direct methods and expanded using Fourier and difference Fourier techniques. Details of crystal parameters and structure refinements are given in Table 4. Selected bond lengths and angles of [**1**][$PF_6$]$_2$·3$H_2O$, **2**, and [**3**]·$CH_3OH$·$H_2O$ are shown in Tables S1, S2, and S3, respectively, in the Supporting Information. ORTEP[18] was used to plot the molecular structures.

CCDC-800550 (for [**1**][$PF_6$]$_2$·3$H_2O$), -800551 (for **2**), and -800552 (for [**3**]·$CH_3OH$·$H_2O$) contain the supplementary crystallographic data for this paper. These data can be obtained free of charge from The Cambridge Crystallographic Data Centre via http://www.ccdc.cam.ac.uk/data_request/cif.

**Details of the Theoretical Calculations:** All calculations were carried out by DFT methods with the B3LYP functional by using the Gaussian 03 programs.[19] For the calculation on [**1**]$^{2+}$ and **3**, the crystal data of [**1**][$PF_6$]$_2$·3$H_2O$ and [**3**]·$CH_3OH$·$H_2O$, respectively, obtained in this study were used. The data of [**4**][PF]$_2$[4a,5] available in the literature were used for the calculation on [**4**]$^{2+}$. The structures of **2a** and [**5**]$^{2+}$, the crystal structures of which are not available, were optimized by using the crystal structures of polymeric *trans*(μ-O,CN)-[$Ru_2$(μ-O)(μ-$CH_3COO$)$_2$(bpy)$_2$(CN)$_2$] (**2**) and *trans*(μ-O,mim)-[$Ru_2$(μ-O)(μ-$CH_3COO$)$_2$(bpy)$_2$(mim)$_2$][PF]$_2$ (mim = *N*-methylimidazole),[7d] respectively, as structural models. The ground state was calculated under the spin-restricted assumption. The components of MOs were analyzed on the basis of natural atomic orbitals.[20] To obtain the information about electronic transitions, several lowest excited states were calculated by using time-dependent (TD)-DFT methods. For graphical displays, the GaussView[21] and GaussSum[22] programs were used.

**Supporting Information** (see footnote on the first page of this article): Crystallographic data in CIF; tables showing the bond lengths and angles of three complexes; tables showing Mulliken population of MOs for **2a** and **3**; and tables showing the energy, oscillator strength, and major contribution of calculated transitions for [**1**]$^{2+}$, **2a**, **3**, [**4**]$^{2+}$, and [**5**]$^{2+}$; and figures showing the calculated spectra for the five complexes.

## Acknowledgments

This work was financially supported by a Grant-in-Aid for Scientific Research from the Ministry of Education, Science, Sports, and Culture of Japan. H.-X. Z. is grateful to the Japan Society for the Promotion of Science for a postdoctoral fellowship. M. A. acknowledges the financial support from a Grant-in-Aid for Scientific Research on Innovative Areas ("Coordination Programming" Area 2107, grant number 22108523) and the Global COE Program, "Science for Future Molecular Systems", from the Ministry of Education, Culture, Sports, Science and Technology of Japan.

[1] a) I. V. Korendovych, S. V. Kryatov, E. V. Rybak-akimova, *Acc. Chem. Res.* **2007**, *40*, 510–521; b) L. Que Jr., Y. Dong, *Acc. Chem. Res.* **1996**, *29*, 190–196; c) W. H. Armstrong, A. Spool, G. C. Papaefthymiou, R. B. Frankel, S. J. Lippard, *J. Am. Chem. Soc.* **1984**, *106*, 3653–3667.

[2] a) R. Manchanda, G. W. Brudvig, R. H. Crabtree, *Coord. Chem. Rev.* **1995**, *144*, 1–38; b) K. Wieghardt, *Angew. Chem.* **1989**, *101*, 1179; *Angew. Chem. Int. Ed. Engl.* **1989**, *28*, 1153–1172.

[3] a) M. Abe, A. Inatomi, Y. Hisaeda, *Dalton Trans.* **2011**, *40*, 2289–2298; b) F. Liu, T. Cardolaccia, B. J. Horstein, J. R. Schoonover, T. J. Meyer, *J. Am. Chem. Soc.* **2007**, *129*, 2446–2447; c) J. L. Chen, L. Y. Zhang, Z. N. Chen, L. B. Gao, M. Abe, Y. Sasaki, *Inorg. Chem.* **2004**, *43*, 1481–1490; d) T. Ito, T. Hamaguchi, H. Nagino, T. Yamaguchi, J. Washington, C. P. Kubiak, *Science* **1997**, *277*, 660–663; e) Y. Arikawa, N. Matsumoto, T. Asayama, K. Umakoshi, M. Onishi, *Dalton Trans.* **2011**, *40*, 2148–2250; f) J. R. Houston, M. M. Olmstead, W. H. Casey, *Inorg. Chem.* **2006**, *45*, 7799–7805; g) K. Wieghardt, M. Koppen, B. Nuber, J. Weiss, *J. Chem. Soc., Chem. Commun.* **1986**, 1530–1532; h) H. Sugimoto, K. Kitayama, K. Ashikari, C. Matsunami, N. Ueda, K. Umakoshi, Y. Hosokoshi, Y. Sasaki, S. Itoh, *Inorg. Chem.* **2011**, *50*, 9014–9023.

[4] a) Y. Sasaki, M. Suzuki, A. Tokiwa, M. Ebihara, T. Yamaguchi, C. Kabuto, T. Ito, *J. Am. Chem. Soc.* **1988**, *110*, 6251–6252; b) H. Kobayashi, N. Uryu, I. Mogi, Y. Sasaki, Y. Ohba, M. Iwaizumi, T. Ochi, A. Ohto, T. Yamaguchi, T. Ito, *Bull. Pol. Acad. Sci. Chem.* **1994**, *42*, 455–465; c) P. Neubold, K. Wieghardt, B. Nuber, J. Weiss, *Angew. Chem.* **1988**, *100*, 990; *Angew. Chem. Int. Ed. Engl.* **1988**, *27*, 933–935; d) M. C. Bar-

  

ral, R. Jimenez-Aparicio, E. C. Royer, F. A. Urbanos, A. Monge, C. Ruiz-Valero, *Polyhedron* **1991**, *10*, 113–120; e) M. C. Barral, R. Jimenez-Aparicio, R. Kramolowsky, I. Wagner, *Polyhedron* **1993**, *12*, 903–910; f) B. K. Das, A. R. Chakravarty, *Inorg. Chem.* **1990**, *29*, 2078–2083; g) A. Syamala, M. Nethaji, A. R. Chakravarty, *Inorg. Chim. Acta* **1995**, *229*, 33–38; h) A. Syamala, A. R. Chakravarty, *Polyhedron* **1994**, *13*, 3079–3083; i) A. Syamala, A. R. Chakravarty, *Polyhedron* **1993**, *12*, 1545–1552; j) C. Sudha, S. K. Mandal, A. R. Chakravarty, *Inorg. Chem.* **1998**, *37*, 270–278; k) A. Syamala, B. K. Das, A. R. Chakravarty, *Polyhedron* **1992**, *11*, 335–339; l) C. Sudha, S. K. Mandal, A. R. Chakravarty, *Inorg. Chem.* **1993**, *32*, 3801–3802; m) J. M. Santos, C. Cipriano, R. B. Faria, J. D. Figueroa-Villar, *Can. J. Chem.* **1997**, *75*, 890–898; n) A. Llobet, M. E. Curry, H. T. Evans, T. J. Meyer, *Inorg. Chem.* **1989**, *28*, 3131–3137; o) H. Uehara, T. Inomata, M. Abe, K. Uosaki, Y. Sasaki, *Chem. Lett.* **2008**, *37*, 684–685; p) A. V. Eremin, A. N. Belyaev, S. A. Simanova, *Russ. J. Coord. Chem.* **2005**, *31*, 761–767; q) J. M. Santos, A. L. B. Formiga, J. D. Figueroa-Villar, *J. Mol. Struct.* **2002**, *608*, 143–149; r) J. F. Ojo, Y. Hasegawa, Y. Sasaki, K. Kunimasa, M. Abe, N. Ohta, *Inorg. React. Mech.* **2000**, *2*, 301–311; s) J. M. Santos, R. Ribeiro da Silva, A. L. B. Formiga, L. W. Tinocp, J. D. Figueroa-Villar, *Chem. Phys.* **2004**, *306*, 143–151; t) R. S. Hussain, R. B. Shukla, H. J. Padhiyar, K. N. Bhatt, *J. Mol. Catal. A* **2003**, *193*, 1–12.

[5] Y. Sasaki, M. Suzuki, A. Nagasawa, A. Tokiwa, M. Ebihara, T. Yamaguchi, C. Kabuto, T. Ochi, T. Ito, *Inorg. Chem.* **1991**, *30*, 4903–4908.

[6] a) M. Valli, S. Miyata, H. Wakita, T. Yamaguchi, A. Kikuchi, K. Umakoshi, T. Imamura, Y. Sasaki, *Inorg. Chem.* **1997**, *36*, 4622–4626; b) N. Gupta, S. Mukerjee, S. Mahapatra, M. Ray, R. Mukherjee, *Inorg. Chem.* **1992**, *31*, 139–141; c) T. Tanase, N. Takeshita, S. Yano, I. Kinoshita, A. Ichimura, *New J. Chem.* **1998**, *22*, 927–929; d) T. Tanase, N. Takeshita, C. Inoue, M. Kato, S. Yano, K. Sato, *J. Chem. Soc., Dalton Trans.* **2001**, 2293–2302; e) T. Fukumoto, A. Kikuchi, K. Umakoshi, Y. Sasaki, *Inorg. Chim. Acta* **1998**, *283*, 151–159.

[7] a) A. Kikuchi, T. Fukumoto, K. Umakoshi, Y. Sasaki, A. Ichimura, *J. Chem. Soc., Chem. Commun.* **1995**, 2125–2126; b) Y. Sasaki, K. Umakoshi, T. Imamura, A. Kikuchi, A. Kishimoto, *Pure Appl. Chem.* **1997**, *69*, 205–210; c) P. Neubold, K. Wieghardt, B. Nuber, J. Weiss, *Inorg. Chem.* **1989**, *28*, 459–467; d) C. Sudha, A. R. Chakravarty, *J. Chem. Soc., Dalton Trans.* **1996**, 3289–3292.

[8] A. Hassain, A. K. Bhatt, D. K. Kumar, R. B. Thorat, H. J. Padhiyar, R. S. Shukla, *Inorg. Chim. Acta* **2009**, *362*, 1101–1108.

[9] a) T. Ochi, Y. Sasaki, T. Yamaguchi, T. Ito, *Chem. Lett.* **1991**, 2019–2022; b) M. Abe, A. Mitani, A. Ohsawa, M. Herai, M. Tanaka, Y. Sasaki, *Inorg. Chim. Acta* **2002**, *331*, 158–167; c) A. Syamala, A. R. Chakravarty, *Inorg. Chem.* **1991**, *30*, 4699–4704.

[10] F. A. Cotton, G. Wilkinson, *Advanced Inorganic Chemistry*, 5th ed., Wiley, New York, **1988**, p. 253.

[11] a) H. Sawamoto, *Master Thesis*, Saitama University, **2000**; b) H. Uehara, M. Abe, Y. Hisaeda, K. Uosaki, Y. Sasaki, *Chem. Lett.* **2006**, *35*, 1178–1179.

[12] Despite the difference of the Ru–CN bond lengths, the C–N distances are similar between **2** (1.10–1.20 Å) and **3** [1.155(7) and 1.144(9) Å]. Although it may not be significant, a more favorable back-bonding interaction of **3** would be relevant. Also, the weaker Ru–CN bond of **2** might be counterbalanced by the coordination of the other end of the cyanide ligands to $Ag^+$ ion.

[13] K. Nakamoto, *Infrared and Raman Spectra of Inorganic and Coordination Compounds*, 4th ed., Wiley, New York, **1986**.

[14] M. Sano, H. Kashiwagi, H. Yamatera, *Inorg. Chem.* **1982**, *21*, 3837–3841.

[15] *Crystal Clear*, Rigaku Corp., Tokyo, **1999**.

[16] *CrystalStructure 3.8*, Crystal Structure Analysis Package, Rigaku and Rigaku/MSC, 9009 New Trails Dr., The Woodlands, TX 77381, USA, **2000–2006**.

[17] *SHELXL-97*: G. M. Sheldrick, *Acta Crystallogr., Sect. A* **2008**, *64*, 112–122.

[18] Ortep3 for Windows®, v.2.0: L. J. Farrugia, *J. Appl. Crystallogr.* **1997**, *30*, 565–565.

[19] M. J. Frisch, G. W. Trucks, H. B. Schlegel, G. E. Scuseria, M. A. Robb, J. R. Cheeseman, J. A. Montgomery Jr., T. Vreven, K. N. Kudin, J. C. Burant, J. M. Millam, S. S. Iyengar, J. Tomasi, V. Barone, B. Mennucci, M. Cossi, G. Scalmani, N. Rega, G. A. Petersson, H. Nakatsuji, M. Hada, M. Ehara, K. Toyota, R. Fukuda, J. Hasegawa, M. Ishida, T. Nakajima, Y. Honda, O. Kitao, H. Nakai, M. Klene, X. Li, J. E. Knox, H. P. Hratchian, J. B. Cross, V. Bakken, C. Adamo, J. Jaramillo, R. Gomperts, R. E. Stratmann, O. Yazyev, A. J. Austin, R. Cammi, C. Pomelli, J. W. Ochterski, P. Y. Ayala, K. Morokuma, G. A. Voth, P. Salvador, J. J. Dannenberg, V. G. Zakrzewski, S. Dapprich, A. D. Daniels, M. C. Strain, O. Farkas, D. K. Malick, A. D. Rabuck, K. Raghavachari, J. B. Foresman, J. V. Ortiz, Q. Cui, A. G. Baboul, S. Clifford, J. Cioslowski, B. B. Stefanov, G. Liu, A. Liashenko, P. Piskorz, I. Komaromi, R. L. Martin, D. J. Fox, T. Keith, M. A. Al-Laham, C. Y. Peng, A. Nanayakkara, M. Challacombe, P. M. W. Gill, B. Johnson, W. Chen, M. W. Wong, C. Gonzalez, J. A. Pople, *Gaussian 03*, rev. C.02, Gaussian, Inc., Wallingford CT, **2004**.

[20] E. D. Glendening, A. E. Reed, J. E. Carpenter, F. Weinhold, *QCPE Bull.* **1990**, *10*, 58.

[21] *GaussView 3.0*, Gaussian, Inc., Wallingford CT, **2000**.

[22] N. M. O'Boyle, A. L. Tenderholt, K. M. J. Langner, *Comput. Chem.* **2008**, *29*, 839–845.

Received: July 13, 2011
Published Online: October 21, 2011

  